

# MATLAB modelling of double sided photovoltaic cell module

Research Article

Yan Zhen<sup>1,\*</sup>, Wu Zuyu<sup>2</sup>, Zhu Ninghui<sup>3</sup>, Yuan Ligen<sup>1</sup>, Chen jing yu<sup>1</sup>

<sup>1</sup>China University of Mining and Technology, Xuzhou City, Jiangsu Province 221116, China

<sup>2</sup>York University, Yorkshire, UK, YO10 5DD, China

<sup>3</sup>State Grid NARI Group China Power Purui Power Engineering Co., Ltd., Changping District, Beijing 102200, China

Received: March 16, 2021; Accepted: April 29, 2021

**Abstract:** In this paper, the equatorial coordinate system is taken as the celestial coordinates, the double-sided photovoltaic module irradiance model is established by using the MATLAB simulation software, and the double-sided photovoltaic module irradiance model is combined with the photovoltaic module model (Jianhui (2001)) to form the mathematical model of the real-time generation system of double-sided photovoltaic modules. The effectiveness of the simulation model was verified by building an experimental platform, and the output characteristics of the optimal line spacing between the double-sided p-v module and the single-sided p-v module were further tested and compared.

**Keywords:** double sided photovoltaic module • back irradiance • modelling • output characteristics • MPPT

## 1. Introduction

Different from the traditional monofacial photovoltaic cells (mPV) with an opaque back sheet, bifacial photovoltaic cells (bPV) have a transparent back sheet that can absorb sunlight to generate electricity. Although the manufacturing cost of bPV is slightly higher than mPV, the power generation efficiency is greatly improved, and this fact has attracted extensive attention from scientific researchers.

Compared with mPV modules, both front and back sides of bPV modules can use tempered glass as a protective material, which provides adequate lighting, weather resistance and high reliability Wu et al. (2020). The power gain on the back can significantly increase the power generation efficiency per unit area. The installation methods are also diversified, which can be both vertical and tilttable. Therefore, it can be used in many locations, such as greenhouses, highway fences, sunrooms, lakes, grasslands etc. (Shiqin, 2019).

Currently, the irradiance modelling of bPV is still mainly based on the mPV irradiance model, which takes the sum of the irradiance of the front and back panels into consideration. Either the equatorial coordinate system or the horizon coordinate system can be adopted by the celestial coordinate system of the irradiance model. Generally, the horizontal solar irradiance outside the atmosphere is calculated according to the zenith angle. Then, the hourly solar irradiance is calculated by the hourly clearness coefficient. Finally, the omnidirectional irradiance of the inclined surface of the photovoltaic (PV) module can be calculated by using the solar incident angle. The irradiance model of the bPV back sheet mainly includes scattered irradiance and ground reflection irradiance. According to whether the scattered irradiance is equal in all directions, irradiance can be divided into sky isotropy and sky anisotropy Perez (1990). Due to the impact of the bPV bracket, the backscattered irradiance belongs to the sky anisotropy, and the integral equation of the correction factor for the scattering incident angle can be obtained by using numerical methods (Marion, 2017). Also, a configuration coefficient is introduced to quantify the complex effect of back shadow. First, the rear surface is divided into 180 equal-area blocks. Then, assuming the shadow area in each block is also

\* Email: 470673627@qq.com

equal, the irradiance of each part is corrected by the incident angle multiplied by the corresponding configuration coefficient. Finally, the backscattered irradiance can be obtained by superimposing the corrected irradiance from each block (Marion et al., 2017). The high-speed feature of the modelling method makes it suitable for large-scale power generation components. As for small-scale components, the method of distinguishing positions along the length of the part can be used (Lorenzo et al., 1985; Yusufoglu et al., 2014). However, this method is characterised by high modelling complexity and is computationally expensive.

This study mainly introduces the modelling and characteristics of bPV modules, and its power generation under shading, which use the MATLAB/SIMULINK simulation to establish a bPV irradiance model and a bPV model. It is later combined as a real-time bPV power generation model. The bPV model proposed in this study is not only easy to operate, but also accurate. Initially, based on the declination angle, zenith angle and incident angle, the direct frontal irradiance, scattered irradiance and ground reflected irradiance, respectively, were determined, which will effectively establish a calculation module for total irradiance. Then, a  $4 \times 4$  bPV array is built and its horizontal and vertical shading are compared, and the power generation efficiency is observed under different shading conditions. Finally, an experiment is conducted to verify its accuracy, and it is worth noting that the PV modules in the experiment are based on the optimal row spacing.

## 2. Modelling of bPV Modules

It is necessary to determine the frontal irradiance model initially. The model is a gradual process. It firstly introduces the solar radiation from outside the atmosphere to the horizontal plane before directing radiation into the inclined plane of the module. The analysis of surface illumination is shown in Figure 1. According to Jianbo (2014), for the calculation formula of the model, parameters such as the declination angle ( $\delta$ ), zenith angle ( $\theta_z$ ) and incident angle (solar elevation angle  $\alpha$ , azimuth  $\gamma_s$ ) are needed, which are shown in Eqs (1)–(4).

$$\delta = 23.45 \sin[2\pi(n+284)/365] \quad (1)$$

$$\cos\theta_z = \cos\varphi\cos\delta\cos\omega + \sin\varphi\sin\delta \quad (2)$$

$$\sin\alpha = \sin\varphi\sin\delta + \cos\varphi\cos\delta\cos\omega \quad (3)$$

$$\sin\gamma_s = \cos\delta\sin\omega / \cos\alpha \quad (4)$$

where  $n$  is one day of a year,  $\varphi$  is the latitude ( $^\circ$ ) and  $\omega$  is the solar hour angle ( $^\circ$ ).

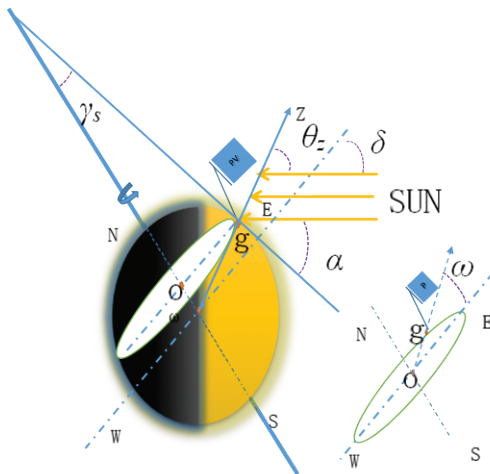


**Fig. 1.** Surface lighting.

Then, the total irradiance ( $I$ ) model requires the irradiance model outside the atmosphere ( $I_0$ ) to be established and combined with the solar irradiance coefficient ( $k_T$ ) Hong (2020), and the model can be expressed by Eqs (5)–(8).

$$I = \varepsilon I_s \cos \theta_z k_T \quad (5)$$

$$\varepsilon = 1 + 0.033 \cos(2\pi n / 365) \quad (6)$$

$$k_T = I / I_0 \quad (7)$$

$$I_d / I = \begin{cases} 1 - 0.09k_T & , \quad k_T \leq 0.22; \\ 0.9511 - 0.1604k_T + 4.388k_T^2 - 16.638k_T^3 & , \quad 0.22 < k_T \leq 0.8; \\ 0.165 & , \quad k_T > 0.8. \end{cases} \quad (8)$$

where  $I_s$  is the solar constant ( $\text{W}/\text{m}^2$ ), which is  $1,367 \text{ W}/\text{m}^2$ ,  $\varepsilon$  is the earth orbit eccentricity correction factor and  $I_d$  is the hourly scattered irradiance ( $\text{W}/\text{m}^2$ ).

Finally, by considering the tilt angle of the module, the direct frontal irradiance, scattered irradiance and ground reflected irradiance of the double-sided module are established, respectively. The three parallel sky anisotropic irradiance models are added together to obtain the total frontal irradiance model (Zhang et al., 2020). The formulas are stated as follows:

$$I = I_b + I_d \quad (9)$$

$$\frac{I_{b,T} \cos \theta_z}{I_b} = \sin \delta \sin \varphi \cos \beta - \sin \delta \cos \varphi \sin \beta \cos \gamma + \cos \delta \cos \varphi \cos \beta \cos \omega + \cos \delta \sin \varphi \sin \beta \cos \gamma \cos \omega + \cos \delta \sin \beta \sin \gamma \sin \omega \quad (10)$$

$$I_T = (I_b + I_d I_b / I_0) I_{b,T} / I_b + I_d (1 - I_b / I_0) [1 + (1 + \cos \beta) / 2] [1 + (I_b / I)^{0.5} \sin^3(\beta / 2)] + I \rho (1 - \cos \beta) / 2 \quad (11)$$

$$I_{\text{BIFI}} = I_{\text{FRONT}} + I_{\text{BACK}} \times \lambda \quad (12)$$

where  $I_b$  is horizontal plane irradiance ( $\text{W}/\text{m}^2$ ),  $I_{b,T}$  is the hourly direct irradiance of inclined surface ( $\text{W}/\text{m}^2$ ),  $\rho$  is ground reflectivity,  $\beta$  is the tilt angle of PV modules ( $^\circ$ ) and  $\lambda$  is the double-side coefficient.

The backside is equivalent to the inversion of the front side. Namely, the tilt angle is increased by  $180^\circ$  and is input to the backside irradiance (BSI) model. By combining the front side irradiance (FSI) module, the total irradiance will be obtained as shown in (12). However, the simulation shows that the BSI module is based solely on the sky anisotropic model, which has negative values in the direct irradiance part. The reason is that the coordinate system used for modelling is a transparent body, whereas Earth is a physical entity with a limited direct angle. It is not possible for solar irradiance to penetrate the Earth continuously to achieve a direct angle to the PV panels. Therefore, it is necessary to consider whether the direct solar irradiance can be collected from the back side of bPV. By observation, besides the time of sunrise and sunset, we can infer it is not possible for the sun to shine directly on the backside.

The simulation is focused on the period between sunrise and sunset. Therefore, the azimuth of sunrise and sunset are needed to make a determination, which is shown in Eqs (13)–(15). Among them, Eq. (15) is for solar time angle, where it is converted into radians. By combining the value of sunrise and sunset, the model of bPV generation is established, which is shown in Figure 2. As a result, the direct irradiance on the backside is limited to the direct angle, and its value is zero at sunrise and sunset.

$$\cos \omega_{s,r} = \tan \varphi \tan \delta \quad (13)$$

$$\omega_{s_r} = -\omega_{s_s} \quad (14)$$

$$t = \frac{\omega \times 180}{\delta \times 15} + 12 \quad (15)$$

where  $\omega_{s_r}$  is the azimuth of sunrise ( $^\circ$ ),  $\omega_{s_s}$  is the azimuth of sunset ( $^\circ$ ), and  $t$  is the solar time (h).

Based on the model of the total irradiance of bPV in Figure 2, and referring to the PV mathematical model in Van Kerschaver et al. (2000), the power generation model of bPV modules are made, which are shown in Figure 3. As the components are connected in series, the equivalent current source is connected in parallel with a reverse diode. Unlike the diode in the equivalent circuit, this diode is a freewheeling diode that prevents short-circuiting of the current source under irregular shadows.

The power loss of double-sided photovoltaic under the equivalent shading effect was ( $\eta_{\text{loss}}$ ):

$$\eta_{\text{loss}} = \frac{P_{\text{unshade}} - P_{\text{shade}}}{P_{\text{unshade}}} \times 100\% \quad (15)$$

where  $P_{\text{unshade}}$  is no shadow maximum power and  $P_{\text{shade}}$  is maximum power under shadow action.

$$SR_{\text{eq}} = \frac{SR_{\text{front}} \times G_{\text{front}}}{G_{\text{front}} + G_{\text{rear}} \times \lambda} \quad (16)$$

where the two-sided coefficient  $\lambda$  is:

$$\lambda = \text{Min}(\lambda_{I_{sc}}, \lambda_{P_{\text{max}}}) \quad (17)$$

$$\lambda_{I_{sc}} = \frac{I_{sc\text{-rear}}}{I_{sc\text{-front}}} \quad (18)$$

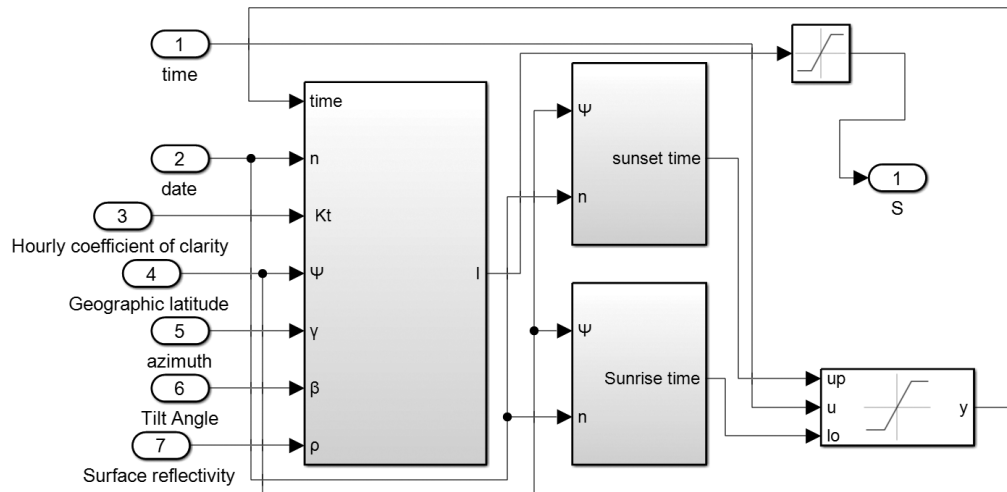


**Fig. 2.** Modelling of total irradiance of components during sunrise and sunset.

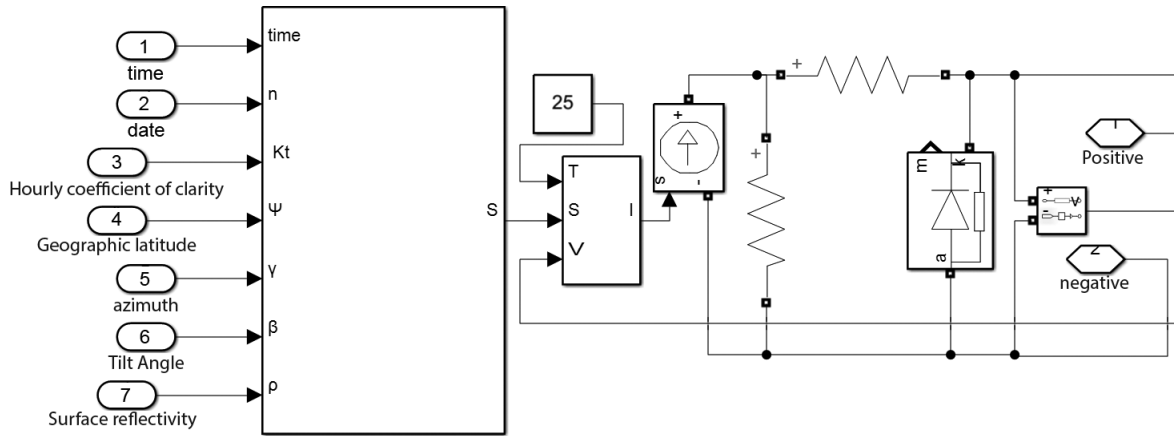


**Fig. 3.** Generation modelling of bPV components. bPV, bifacial photovoltaic cells.

$$\lambda_{p_{\max}} = \frac{P_{\max\text{-rear}}}{P_{\max\text{-front}}} \quad (19)$$

where  $SR_{\text{eq}}$  – equivalent occlusion rate of double-sided components;  $SR_{\text{front}}$  – front occlusion rate of double-sided components;  $G_{\text{front}}$ ,  $G_{\text{rear}}$  – front and back irradiance of double-sided components (the measured results are 810  $\text{W}/\text{m}^2$  and 155  $\text{W}/\text{m}^2$ , respectively);  $I_{\text{sc-front}}$  and  $I_{\text{sc-rear}}$  – the short-circuit current of the front and back sides of the double-sided components under standard conditions (the measured results are 1.63 A and 1.54 A, respectively);  $P_{\max\text{-front}}$  and  $P_{\max\text{-rear}}$  – maximum power under standard conditions on the front and back of double-sided components (the measured results are 14.9 W and 14.1 W, respectively).

The optimal spacing for conventional PV  $D_m$  is given by Wu (2020):

$$D_m = \frac{\cos A \times H}{\tan[\sin^{-1}(\sin \varphi \sin \delta + \cos \varphi \cos \delta \cos \omega)]} \quad (20)$$

The optimal spacing for double-sided photovoltaic e is given by:

$$e = \frac{\sqrt{H^2 + D_b^2} + B - H - L^2 - H^2 + 2HL \cos(\theta + 90^\circ) - D_b^2 + 2BD_b \cos(\arctan(\frac{H + L \sin \theta}{L \cos \theta}))}{2D_b} \quad (21)$$

$$B = \sqrt{L^2 + H^2 - 2HL \cos(\theta + 90^\circ)} \quad (22)$$

where  $A$  – solar azimuth;  $\varphi$  – latitude;  $\delta$  – declination;  $H$  – Height of PV;  $L$  – Length of board;  $\omega$  – time of angle and  $\theta$  – Pv module tilt angle.

### 3. Simulation Analysis of bPV Modules

To obtain the output of the simulation model, seven variables that affect the irradiance of the module were tested and examined in this research, and they are number of days of a year, the time of the day, the hourly solar radiance coefficient, geographic latitude, module azimuth, module inclination angle and ground reflectivity (the concrete floor is set to 0.3) (Jiping et al., 2020). These variables are used to test the output characteristics of bPV cells. The used PV module and the simulated fixed value parameters are shown in Tables 1 and 2, respectively.

First, with the number of days in a year as a variable and the rest of the parameters set to fixed values, the simulated yearly day-by-day noon irradiance variation curve is shown in Figure 4. Although the solar irradiance is relatively more sufficient in summer than in winter, a slight decline was witnessed in the middle of summer. The decline is caused by setting the noontime hourly clear factor to a larger value (0.6), resulting in little scattering and relatively large direct radiation. The advantage of bPV lies in the absorption of scattered radiation on the back. When the solar refraction point reaches the Tropic of Cancer in the summer, the zenith angle reduces. Consequently, the amount of direct radiation further occupies the main body, reducing the backside advantage of the bPV. However, it reflects the benefits of backside power generation of bPV modules during the turn of spring and summer and the turn of summer and autumn. The module increases the number of days of maximum irradiance throughout the year.

Second, using the time of the day as a variable and setting the remaining parameters to fixed values, the irradiance variation curve of the module on a certain day of the year (the 70th day) is simulated as shown in Figure 5. From the simulation, it is observed that the irradiance peaks at noon of the day, because the direct radiation is received the most at noontime due to the rotation of the Earth. Moreover, it was observed that the irradiance at sunrise and sunset is not zero. This is because even though no direct radiation is available at this time, a small amount of scattered radiation can still be collected.

Finally, after obtaining the results of annual irradiance, the output characteristics of the bPV array can be calculated in the model, which is according to the model shown in Figure 3. In the simulation, a  $4 \times 1$  bPV array is involved, which is an example to illustrate the output performance. The hourly I–V curve and P–V curve without shading are obtained in Figure 6.

When considering the shading of the bPV array, it can be classified into the longitudinal shading and transverse shading. Figure 7 shows the simulation results of the open circuit voltage and short circuit current of the  $4 \times 4$  bPV array, blocking one row horizontally and one string vertically. According to the results, it can be found that longitudinal shading causes the short circuit current and the open circuit voltage to drop significantly. It is due to the smaller proportion of non-shading, and the transformation of a string of shaded components into a load, which caused the array to not be able to actually work in an open circuit state. For horizontal shielding, the smaller the proportion of non-shielding is, the more gradually does the open circuit voltage decrease, and the short circuit current is basically unchanged, but slightly decreases. It is also because the shading component is turned into a load, and the circuit is not a short circuit.

**Table 1.** bPV module parameters.

$U_{oc}$	$U_{mmp}$	$I_{sc}$	$I_{mmp}$	$P_{max}$
11.48 V	9.34 V	1.63 A	1.61 A	15 W

bPV, bifacial photovoltaic cells.

**Table 2.** Simulation fixed value parameters

day	time	$k_T$	$\varphi$	$\gamma$	$\beta$	$\rho$
70	12	0.6	34°	0°	50°	0.3

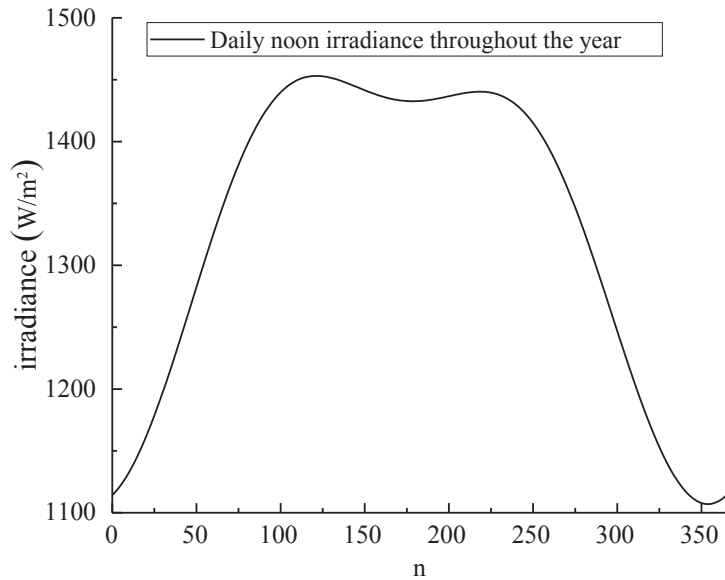


Fig. 4. Simulation of the annual midday daily irradiance of the module.

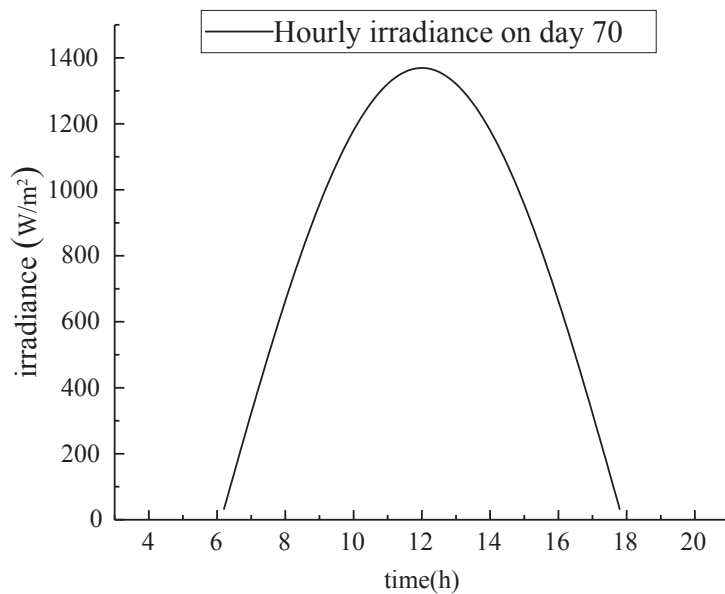


Fig. 5. Hourly irradiance simulation on the 70th day of a year.

## 4. Experiment

The experimental equipment includes: 20 pieces of bPV, 20 pieces of mPV, infrared thermal imager, light intensity measuring instrument, sliding rheostat, Boost circuit, TMS320F28335, etc.

As in Figure 8, 20 bPV modules were included in the experiment platform, with a background made of white plastic plates to increase the intensity of reflected radiation.

First, to verify the accuracy of the simulation, four of the modules were connected in series to test the output characteristics and output power without shading. The simulation results were compared in Figure 9. Due to the different illuminating environment on the backside, a slight irregular shading phenomenon can be observed on the bPV modules.

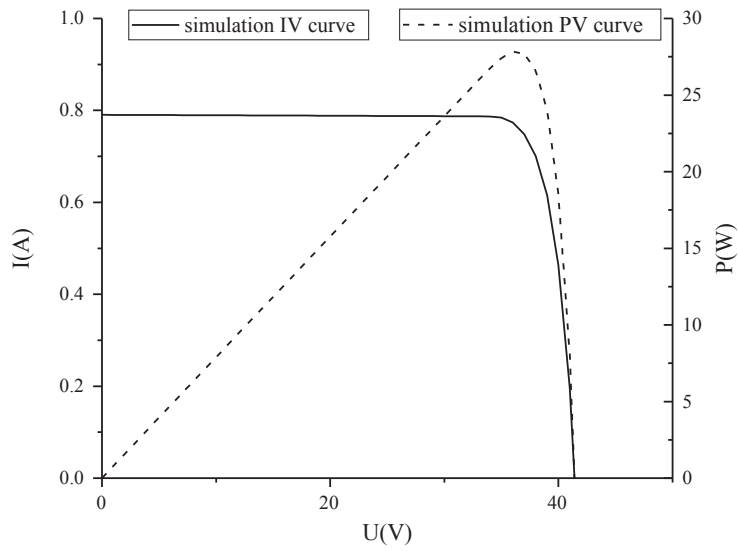


**Fig. 6.** Series simulation of module power generation model.

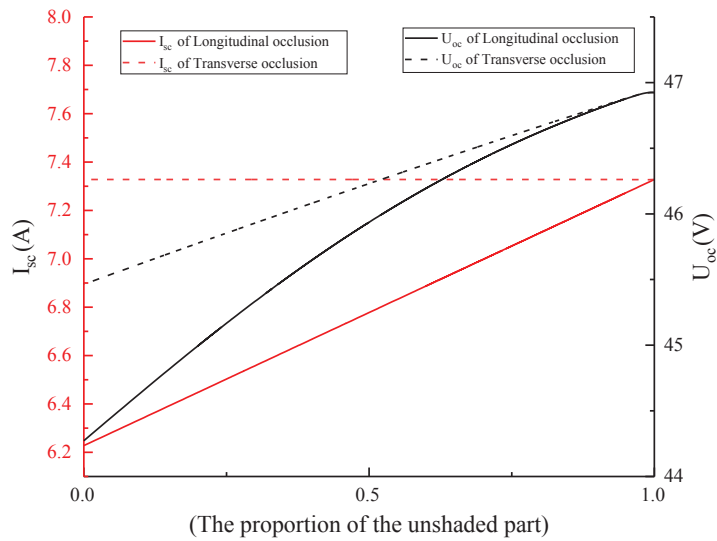


**Fig. 7.** 4 × 4 bPV array occlusion simulation. bPV, bifacial photovoltaic cells.



**Fig. 8.** Physical picture of bPV module. bPV, bifacial photovoltaic cells.



The curves of the change of the open-circuit voltage versus the change of short circuit current under different temperatures are illustrated in Figure 10. It shows that the temperature rises and the open-circuit voltage gradually decreases, while the short circuit current rises slightly. The trend is partly caused by the PN (p-type semiconductor and n-type semiconductor) junction structure inside the PV module, where the majority carrier and the minority carrier tend to be highly active under heating conditions.

To verify the accuracy of the double-sided coefficient ( $\lambda$ ), the power loss of double-sided photovoltaic under the equivalent shading effect was detected ( $\eta_{loss}$ ).

According to Figure 11, the module demonstrates a satisfying performance when the shading rate is <30% and >50%. However, due to the error of measurement, there is a slight discrepancy between 30% and 50%. In this part of the test, the double-sided coefficient is about 0.94, which is used for the equivalent calculation of the back irradiance of the model.

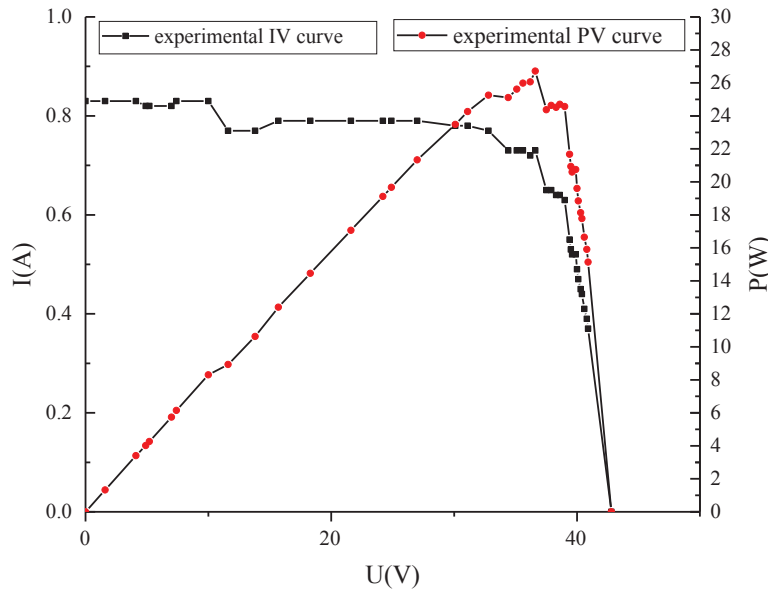


Fig. 9. Experimental output IV and PV curves. IV, Current and voltage . PV, Power and voltage.

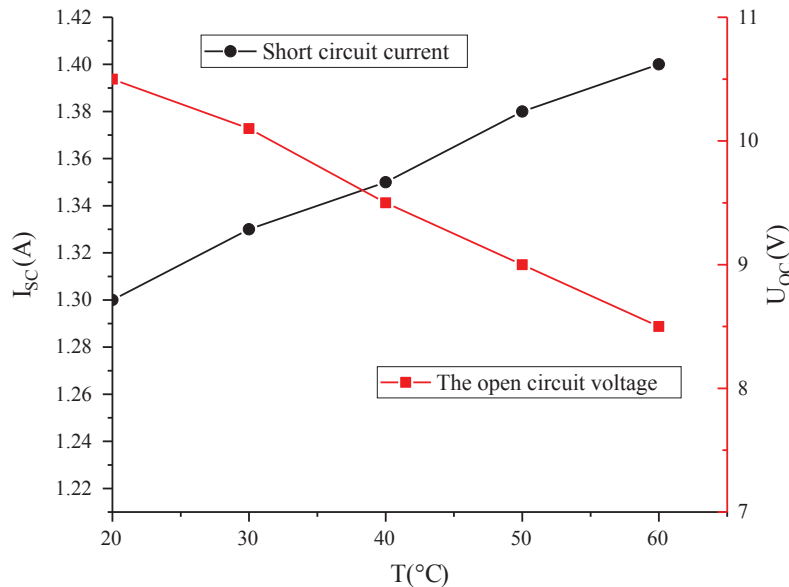


Fig. 10. Effect of temperature on open circuit voltage and short circuit current.

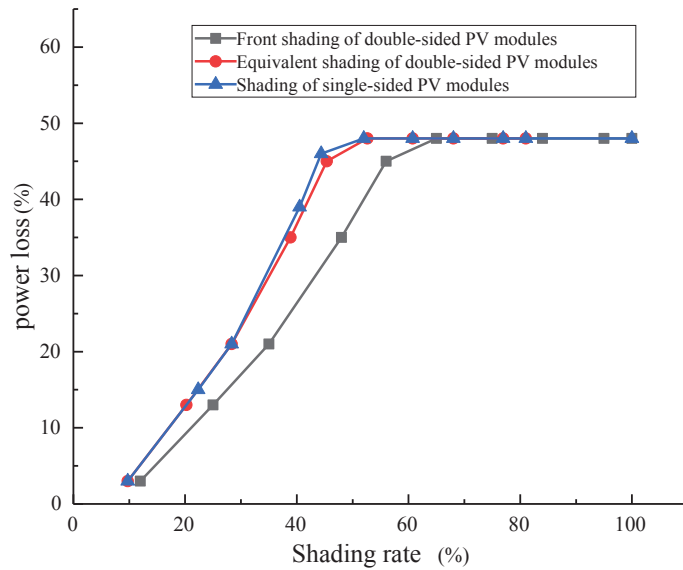


Fig. 11. Comparison of equivalent shading.

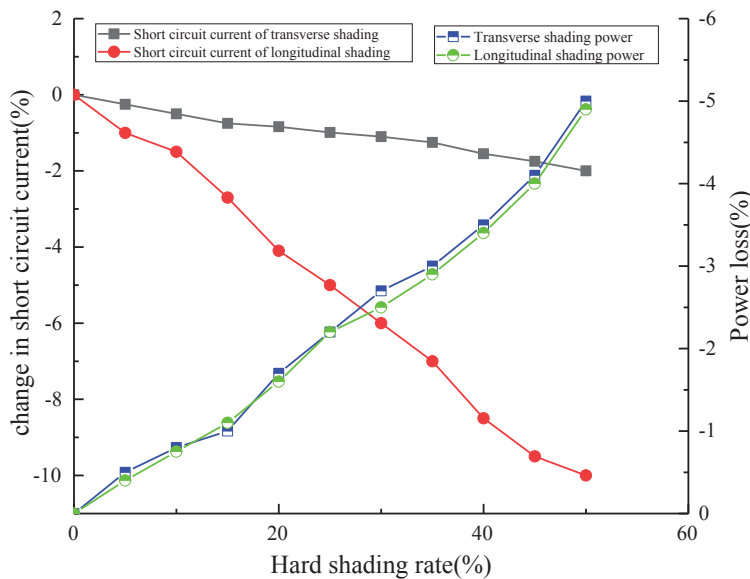


Fig. 12. Variation of short circuit current and power under different shading conditions.

To verify the shading characteristics of bPV module array, a  $4 \times 4$  bPV array is combined. The change of short-circuit current and power is detected under the rigid shading of a bPV panel, which is divided into horizontal shading and vertical shading. The result is shown in Figure 12, where the vertical shading shows a more significant influence on the short-circuit current than the horizontal shading. However, the difference between the two in terms of power is insignificant.

To compare the output characteristics of bPV and mPV under different shading conditions, the following experiments were carried out. The series-parallel  $3 \times 6$  PV array is shown in Figure 13 and the yellow area is the measurement module under the MPPT Chunhua (2011) (Maximum power tracking control) working condition. The results measured under a different shading condition are shown in Figure 14. The results show that the No. 7 module is reversed under the partial shading. The diode is turned off and continuously generates electricity as part of the series connection. When the voltage of the other modules in the same string rises, the MPP (maximum power point) voltage of in the entire array is slightly increased. When full shading happens, the reverse diode of the

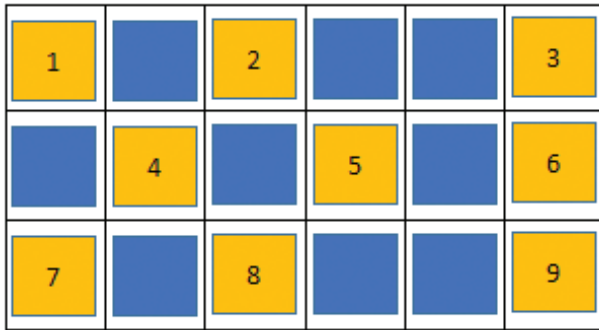


Fig. 13. 3 × 6 PV array. PV, photovoltaic.

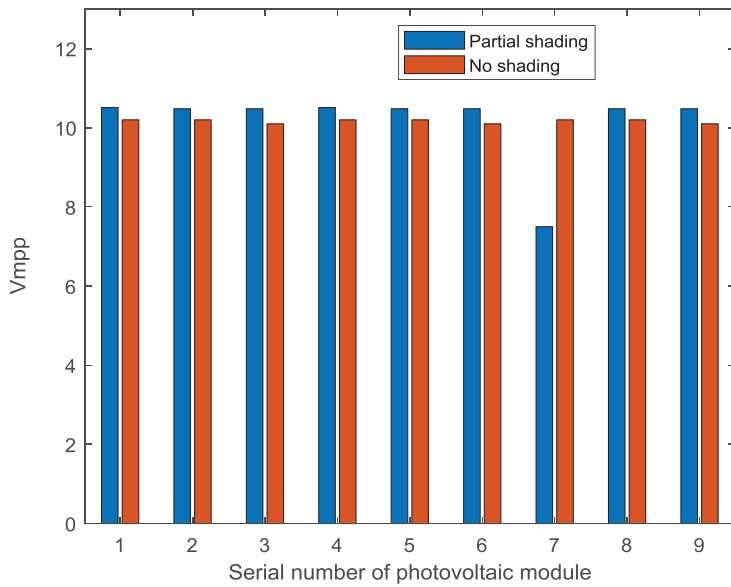


Fig. 14. Incomplete shading No. 7 of bPV component array. bPV, bifacial photovoltaic cells.

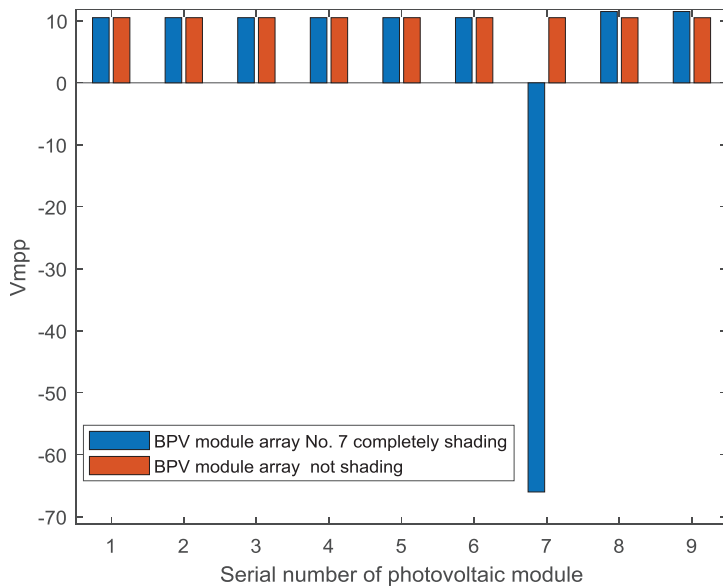
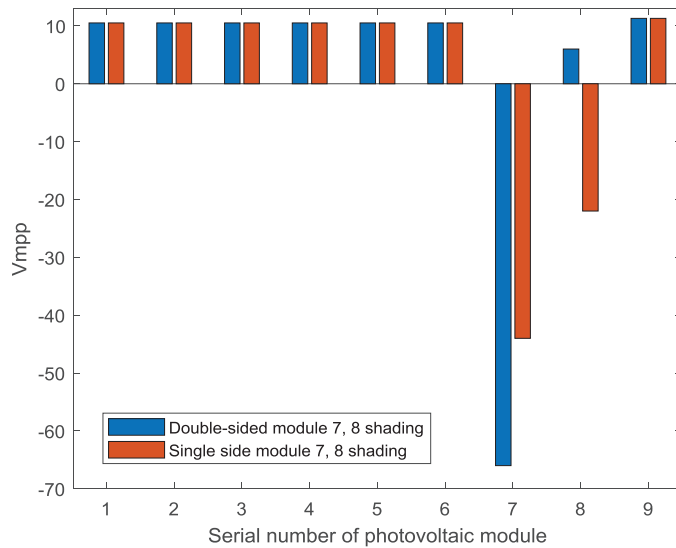


Fig. 15. Fully shaded No. 7 of bPV component array. bPV, bifacial photovoltaic cells.

No. 7 module is turned on and performs as a load in the third string. The voltage of No. 8 and No. 9 modules in the same string is forced to increase while the operation of the other two strings is not affected, as shown in Figure 15. It can be observed that a single bPV module shares the same shading effect of mPV modules Yihui (2016).

The result that follows when the two PV modules of No. 7 and No. 8 are fully shaded on the front side simultaneously is shown in Figure 16. At this time, only No. 7 of the bPV modules is turned into a load while No. 8 is in a low-voltage working state, leading to the voltage rise of the other modules in the same string. The power of the string drops and the other two strings are not affected. This result is inconsistent with mPV modules, where No. 7 and No. 8 are both converted into loads under the condition of full shading. The causes for the inconsistency are analyzed in detail, which is due to the internal resistance and partial pressure. Owing to the different lighting on the back of the bPV, No. 8 can still work, improving the overall power. Meanwhile, No. 7 is in a state of self-consumption power generation Yan (2013).

Now, the power of bPV and mPV under the optimal spacing is compared. According to the formulas forming part of Eqs (20)–(22),  $E = 15\%$ ,  $\theta = 45^\circ$ ,  $L = 0.39$  m, and  $H = 0.34$  m. The optimal row spacing of double-sided array is 1.01 m, and that of single-sided array is 0.79 m; also, the installation array is as shown in Figure 17. Then, the power stability of the mPV array and bPV array with the best spacing under different weather conditions were tested and compared. The result as shown in Figure 18 indicates that the adaptability of the bPV is stronger in the case of bad weather. Also, the comparison of maximum power point of mPV array and bPV array in a day is shown in Figure 19.



**Fig. 16.** No. 7 and No. 8 with full shading on the front of the bPV module array. bPV, bifacial photovoltaic cells.



**Fig. 17.** bPV array optimal spacing test. bPV, bifacial photovoltaic.

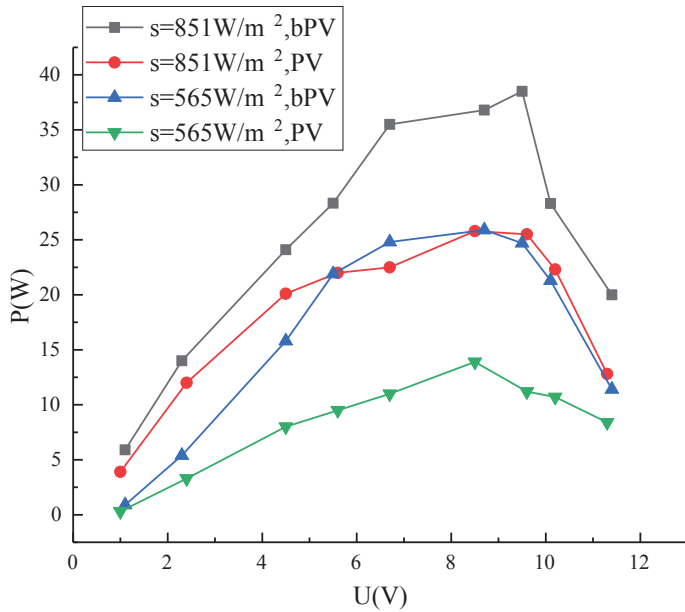


**Fig. 18.** Comparison of power stability of mPV and bPV under different weather conditions. bPV, bifacial photovoltaic cells; mPV, monofacial photovoltaic cells.

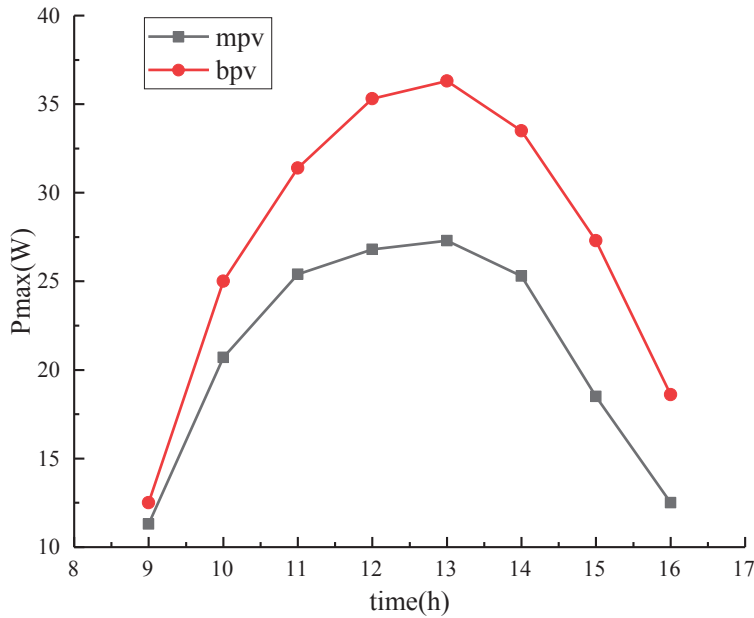


**Fig. 19.** Maximum power comparison of single - and double-sided PV arrays with optimal spacing.

## 5. Conclusion

In this paper, a MATLAB model of a real-time power generation system for double-sided photovoltaic cell modules was studied. The shading experiment was carried out to test the output characteristics of the double-sided modules, and the power outputs of single-sided array and double-sided array were compared according to the optimal spacing formula. It can be found that double-sided photovoltaic modules have higher power generation efficiency and reliability due to their unique power generation mode, and the shading effect of their series output characteristics is slightly different from that of traditional modules.

## References

- Chunhua, W., Kun, X. and Jianming, H. (2011). Research on photovoltaic distributed MPPT based on non inverse buck boost converter. *New Electrical Energy Technology*, 30(04), pp. 84–88.
- Hong, J., Renzu, Z., Pei, Z., Lihua, Z., Xue, S. and Peifa, D. (2020). Study on climatological prediction model of hourly solar irradiance. *Jiangsu Agricultural Science*, 48(11), pp. 275–281.
- Jianbo, B. (2014). Modeling, simulation and optimization of solar photovoltaic system. Electronic Industry Press.
- Jianhui, S., Shijie, Y. and Wei, Z. (2001). Mathematical model for silicon solar cell engineering. *Journal of Solar Energy*, 22(04), pp. 409–412.
- Jiping, Z., Guoqiang, H., Hongbo, L., Xiaojun, Y., Cui, L. and Xiao, Y. (2020). Effects of different ground backgrounds on the power generation performance of double-sided photovoltaic modules. *Acta Solar Energy*, 41(03), pp. 298–304.
- Lorenzo, E., Sala, G., Lopez-Romero, S. and Luque, A. (1985). Diffusing reflectors for bifacial photovoltaic panels. *Solar Cells*, 13(3), pp. 277–292.
- Marion, B. (2017). Numerical method for angle-of-incidence correction factors for diffuse radiation incident photovoltaic modules. *Solar Energy*, 147, pp. 344–348.
- Marion, B., MacAlpine, S., Deline, C., Asgharzadeh, A., Toor, F., Riley, D., Stein, J. and Hansen, C. (2017). A practical irradiance model for bifacial PV modules. *2017 IEEE 44th Photovoltaic Specialist Conference (PVSC), Washington, DC*, pp. 1537–1542.
- Perez, R., Ineichen, P., Seals, R., Michalsky, J. and Stewart, R. (1990). Modeling daylight availability and irradiance components from direct and global irradiance. *Solar Energy*, 44(5), pp. 271–289.
- Shiqin, W. (2019). Design and research of photovoltaic power generation system with double-sided photovoltaic modules. *Solar Energy*, 05, pp. 30–33.
- Van Kerschaver, E., Zechner, C. and Dicker, J. (2000). Double sided minority carrier collection in silicon solar cells. *IEEE Transactions on Electron Devices*, 47(4), pp. 711–717.
- Wu, Z., Hu, Y., Wen, J. X., Zhou, F. and Ye, X. (2020). A Review for solar panel fire accident prevention in large-scale PV applications. *IEEE Access*, 8, pp. 132466–132480. doi: 10.1109/ACCESS.2020.301021.
- Wu, Z., Zhou, Z. and Mohammed, A. (2020). Time-effective dust deposition analysis of PV modules based on finite element simulation for candidate site determination. *IEEE Access*, 8, pp. 1–1. doi: 10.1109/ACCESS.2020.2985158.
- Yan, C., Lina, W. and Kai, S. (2013). An independent photovoltaic power supply system based on analog circuit MPPT technology. *New Electrical Energy Technology*, 32(03), pp. 22–26.
- Yihui, P. and Wei, D. (2016). Comparative study on the performance of two improved variable step MPPT algorithms. *New Electrical Energy Technology*, 35(03), pp. 69–75.
- Yusufoglu, U., Pletzer, U., Koduvelikulathu, L. J., Comparotto, C., Kopecek, R. and Kurz, H. (2014). Analysis of the annual performance of bifacial modules and optimization methods. *IEEE Journal of Photo voltaics*, 5(1), pp. 320–328.
- Zhang, Y., Yu, Y., Meng, F. and Liu, Z. (2020). Experimental investigation of the shading and mismatch effects on the performance of bifacial photovoltaic modules. In *IEEE Journal of Photovoltaics*, 10(1), pp. 296–305. doi: 10.1109/JPHOTOV.2019.2949766.